JTTEE5 10:311-325

Microstructure and Properties of WC-10%Co-4% Cr Spray Powders and Coatings: Part 1. Powder Characterization

L.-M. Berger, P. Ettmayer, P. Vuoristo, T. Mäntylä, and W. Kunert

(Submitted 14 March 2000; in revised form 16 June 2000)

WC-10% Co-4% Cr[1] represents an important composition for thermally sprayed hardmetal-like coatings that are applied when simultaneous wear and corrosion resistance is required. In this paper, four commercially available spray powders obtained by various production techniques (sintering and crushing, agglomeration and plasma densification) were thoroughly characterized using a broad variety of physical and chemical methods, including scanning electron microscopy (SEM), energy-dispersive x-ray (EDX), x-ray diffraction, adsorption, mercury intrusion, and helium pycnometry. Special emphasis is given to the interdependence of the chemical and phase compositions. The cooling rate applied during preparation of the spray powders seems to be responsible for the appearance of equilibrium or nonequilibrium phases, as was established from the investigation of the spray powders after heat treatment at 1000 °C. The amount of Cr added to the composition, 4%, is higher than the solubility limit of chromium in the binder phase in the presence of WC; hence, a second carbide phase is formed. The carbon content determines which carbide phase is formed and how both cobalt and chromium are distributed between the hard and the binder phases. A substantial carbon deficiency leads to nearly complete bonding of both chromium and cobalt into carbide phases. As was shown by differential scanning calorimetry (DSC) experiments, such spray powders do not form a melt in the temperature range up to 1465 °C, while powders containing clearly detectable amounts of metallic cobalt form a melt above 1210 °C.

Keywords carbide phases, chemical composition, nonequilibrium carbide phases, phase composition, spray powder characterization, WC-10%Co-4% Cr

1. Introduction

WC-Co is a standard composite material of the carbide hard phase-metallic binder type used for highly wear-resistant thermally sprayed coatings. However, the corrosion resistance of this composite is insufficient for many applications. In such cases, preference is given to coatings produced from commercially available WC-CoCr spray powders, in which the chromium addition provides an improvement in the corrosion resistance of the metallic binder phase over that of unalloyed WC-Co. The compositions WC-10% Co-4% Cr and WC-6% Co-8% Cr are both of importance for thermal spray applications;[1] however, WC-10% Co-4% Cr is the more widely used of the two. Spray powders having this composition are produced by different techniques.

When the first experimental results of the characterization of the four selected commercial WC-10% Co-4% Cr spray powders investigated in this paper were reported,[2] only a few papers which dealt with coatings of this composition had been found in the literature, just one paper providing a thorough characterization of the spray powder.[3] Since that time, the number of papers on the topic of WC-10% Co-4% Cr coatings has increased enormously.[4–8] This is the reason for extending the in-depth characterization of these four commercial WC-10% Co-4% Cr spray powders. Special emphasis was given to the interdependence of chemical composition, preparation conditions, and the appearance of different phases in the spray powders. Results of fundamental hardmetal research were taken into account. Experimental techniques generally not employed for the characterization of spray powders, such as differential scanning calorimetry (DSC), adsorption, scanning electron microscopy (SEM) investigations of etched cross sections of spray-powder particles, a heat treatment at 1000 °C with subsequent reinvestigations, and others, were used. The results of investigations of coatings sprayed from these powders by atmospheric plasma spraying (APS), high-velocity oxy-fuel spraying (HVOF), and detonation gun spraying (DGS) will be published separately.

2. Composition, Phase Relationships, and Composite Properties

2.1 Composition

Additions of Cr_3C_2 to WC-Co are commonly used in the preparation of sintered hardmetals. However, the aim in using these additions is mostly inhibition of carbide grain growth in

L.-M. Berger, Fraunhofer Institute of Ceramic Technologies and Sintered Materials, Dresden, Germany; **P. Ettmayer,** Institute for Chemical Technology of Inorganic Materials, Vienna University of Technology, Vienna, Austria; **P. Vuoristo** and **T. Mäntylä,** Institute of Materials Science, Tampere University of Technology, Tampere, Finland; and **W. Kunert,** Freiberger NE-Metall GmbH & Co Produktions KG, Freiberg, Germany. Contact e-mail: Lutz.M.Berger@ikts.fhg.de.

[1] If not otherwise stated, all percentages given in this paper are in mass%.

the sintering process and not improvement of the corrosion resistance of the metallic binder. Additions of less than 1% are effective for this purpose.[9]

The addition of Cr_3C_2 to WC-Co in amounts greater than those used for grain growth inhibition leads to metallurgical reactions and the formation of new phases. The same is valid when WC is added to a (Co,Cr) binder alloy. The compositions of these new phases are discussed below.

The composition WC-10% Co-4% Cr corresponds to 76.4% WC-15.8% Co-7.8% Cr per volume. Therefore, the relationship of Co:Cr is 2:1 by volume. The nominal content of bonded carbon is 5.27%.

2.2 Hard Phases

In the well-known binary system W-C, the two stable carbides WC and W_2C, both with a hexagonal structure, exist. An additional phase that is known to exist is the high-temperature cubic WC_{1-x} phase, which was originally discovered in DGS coatings.[10] In the Cr-C system, three stable carbides are known to exist: Cr_3C_2 (orthorhombic), Cr_7C_3 (orthorhombic), and $Cr_{23}C_6$ (cubic).

Chromium can be substituted by tungsten in the different chromium carbides in the following amounts: up to 14 mol.%[11] or 16 mol.%[12] "W_3C_2" in Cr_3C_2, up to 6 mol.%[11] or 7 mol.%[12] "W_7C_3" in Cr_7C_3, and up to 16 mol.%[11] or 20 mol.%[12] "$W_{23}C_6$" in $Cr_{23}C_6$. WC has been reported either not to form solid solutions with Cr_3C_2[11,13] or to form solid solutions with up to 4.7 mol.% "CrC."[12] In cubic WC_{1-x}, however, up to 69.3 mol.% "CrC_{1-x}" can be dissolved,[12] but the resulting phase is not stable at lower temperatures.[11]

The solid solubility of "Cr_2C" in W_2C extends up to 92.3 mol.%.[12] Stecher *et al.*[11] found a linear dependence of the lattice parameters, *a* and *c*, of $(W, Cr)_2C$ on the chromium content up to 80 mol.% "Cr_2C" in their samples prepared at 1350 °C. Rudy and Chang[14] mentioned a splitting of the $(W, Cr)_2C$ solid solution into two phases. Remarkably, Eremenko *et al.*[12] found that, for arc-melted samples in the region W-38 at.% C - Cr-40 at.% C, the lattice parameters are constant in two different ranges of the following compositions: $a = 0.2964$ nm and $c = 0.4676$ nm for 30 to 45 mol.% "Cr_2C" in $(W, Cr)_2C$, and $a = 0.2876$ nm and $c = 0.4532$ nm for 63 to 80 mol.% "Cr_2C" in $(W, Cr)_2C$.

Hinnüber and Rüdiger[13] demonstrated that WC-Cr_3C_2 samples with 5 to 75 mol.% Cr_3C_2 also showed the presence of the $(W, Cr)_2C$ phase together with free carbon resulting from the decomposition of WC. The lattice parameters decreased with increasing chromium content but were found to be dependent on the preparation method.

2.3 Interaction of the Hard Phases with the Cobalt Binder

The simple pseudobinary system WC-Co is characterized by the appearance of an equilibrium between the hard WC phase and the metallic Co binder.[9,15] When a carbon deficiency exists, ternary carbides are formed. These are known as η-carbides of the types M_6C (with the range of composition $W_{4-3}Co_{2-3}C$) and $M_{12}C$ (W_6Co_6C) and as the κ-phase W_3CoC. $W_{4-3}Co_{2-3}C$ appears at the lowest degree of carbon deficiency and W_3Co_3C is the most stable composition.[15]

The investigations of the Co-Cr-C system by Köster and Sperner[16] have shown that additions of carbon to a CoCr alloy lead to the formation of Cr_3C_2, Cr_7C_3, and $Cr_{23}C_6$. The solubility of Co in Cr_3C_2 is negligible, whereas the solubility of Co in Cr_7C_3 and $Cr_{23}C_6$ can reach values of 26 and 20%, respectively. Recent thermodynamic evaluations have confirmed the solubility of Co in the M_7C_3 and $M_{23}C_6$ structures.[17]

Additions of approximately 1% Cr as Cr_3C_2 to WC-Co were detected in the binder phase after sintering or in the η-phase under conditions of carbon deficiency.[18] The solubility limit of Cr in the binder was investigated by Suzuki and Tokomotu[19] for WC-15% Co hardmetals with increasing Cr_3C_2 additions (0 to 10%). This limit was found to depend on the carbon content and had values of 4 and 11% in high- and low-carbon composites, respectively. Additions of Cr_3C_2 beyond the solubility limit of Cr led to the formation of M_7C_3-type carbides. Similar results were obtained by Zackrisson *et al.*,[20] who studied the effect of substitution of WC by Cr_3C_2 (up to 6%) on the microstructures and phase compositions of WC-10% Co model alloys. No Cr_3C_2 was found to be undissolved after sintering, but additions of 1.9% and more led to the formation of a chromium- and cobalt-rich $(Cr, Co, W)_7C_3$ phase whose composition depended on the amount of Cr_3C_2 added. However, this phase was not detectable by x-ray diffraction.

In addition, the results of both papers[19,20] are in good agreement with those of Motitschka *et al.*,[21] who investigated artificial binder alloys containing 0.37 and 0.77% carbon. A maximum solubility of 5% Cr in equilibrium with WC occurred at 1000 °C; at 1250 °C, the solubility limit of Cr rises to at least 12%. When the solubility limit is exceeded, $(Cr, Co, W)_7C_3$ is precipitated. This phase appears if the carbon content of the composition is close to the stoichiometric value, $(W + Cr)/C = 1$.[22] In undercarburized hardmetals, chromium stabilizes the η-phase, which has the composition $(Co, Cr)_3W_3C$.[21,22]

Knotek *et al.*[23] investigated the Co-rich corner of the quarternary Co-Cr-W-C system at constant carbon contents of 0.6 and 1%. A wide area of existence of the cubic (Co, Cr, W) solid solution and the intermetallic σ-phase, as well as the existence of the carbides WC, M_7C_3, $M_{23}C_6$, M_6C, $M_{12}C$, and $M_{28}C$ (χ-phase), and free carbon was established. The decomposition of M_6C into (Co, Cr, W), WC, and free carbon was observed. Metallic Co, M_7C_3, $M_{23}C_6$, and Co_3W_3C phases were detected in Co-Cr-W-C alloys with 40% Co and variations in the chromium (30 and 47%) and carbon contents (2.0 to 4.5% and 3.4 to 5.7% at both chromium levels).[24]

The addition of 4% Co to WC-Cr_3C_2 samples basically did not cause the phase compositions or the properties to be different from those of the binderless samples described above.[13] The $(W, Cr)_2C$ phase was detectable only at Cr_3C_2 contents of 25 mol.% and higher.

Summarizing the results of phase-equilibria investigations reviewed above for an alloy with the nominal composition 86% WC-10% Co-4% Cr with 3.6 to 5.2% C and the balance W, the phases WC, the η-phase $(Co, Cr)_3W_3C$, and a (Co, Cr, W) alloy binder are expected to be in thermodynamic equilibrium. The formation of $(Cr, Co, W)_7C_3$, not $(Co, Cr)_3W_3C$, takes place at higher carbon contents.

2.4 Effect of Chromium Additions on the Properties of Sintered WC-CoCr Parts

There has been only a very limited number of investigations performed on the powder-metallurgical preparation and charac-

terization of sintered parts having a composition equal or nearly equal to WC-10% Co-4% Cr. According to Kny *et al.*,[25] the high degree of undercarburization leads to the occurrence of the brittle η-phases and consequently to a transverse rupture strength that is significantly lower than that of WC-Co alloys. At the same time, the hardness HV30 was similar to and the corrosion resistance in several acidic and alkaline solutions was significantly better than those of WC-6% Co alloys. The addition of chromium as Cr_3C_2 to WC-10% Co results in the formation of alloys with a similar chromium, but higher carbon, content,[20,26] which therefore have a different phase composition.[20] The Cr_3C_2 additions to WC-Co mostly eliminate the tendency for discontinuous carbide grain growth, while practically having no influence on the hardness and improving the corrosion resistance in acids.[26] Ninham and Levy[27] found that the erosion resistance of WC-10% Co-4% Cr was significantly higher than that of WC-Co. This was attributed to a solid solution formed by the metals or precipitation of chromium carbides. The more probable reason for this behavior, an increase in the amount of carbides caused by the η-phase formation, apparently was not recognized.

2.5 Investigations of the Spray Powders

In this section, investigations on the characterization of WC-10% Co-4% Cr spray powders found in the literature are briefly reviewed, with emphasis on the chemical and phase compositions.

Guilemany *et al.*[3,28] characterized the commercial sintered and crushed powder Amdry 5843 (Sulzer Metco). They found a total carbon content of 5.39%. They interpreted the peaks detected by x-ray diffraction as being indicative of the presence of WC, Co_3W_3C, and $Cr_{23}C_6$[28] (or Cr_7C_3 in Ref 3). In the case of $Cr_{23}C_6$ or Cr_7C_3, they based this conclusion on only one peak at $2\theta = 44.1°$ (Cu K_α radiation). However, transmission electron microscopy and wavelength dispersive spectroscopy (WDS) investigations led them to conclude that four phases were present: WC, Co_3W_3C, $Cr_{23}C_6$, and metallic Co.

Jacobs *et al.*[7] also characterized the commercial Amdry 5843 powder and found a total carbon content of 5.31%. Using x-ray diffraction, they detected WC, the η-phase $(Co, W)_6C$ with lines shifted to smaller lattice parameters, and Cr_7C_3, which, however, was also identified by one peak only. Using the backscattered electron mode of SEM, they detected two "binder" phases (a cobalt-rich and a chromium-rich phase) besides WC in the spray-powder particles.

Schwetzke and Kreye[4] characterized a sintered and crushed powder and a sintered powder with total carbon contents of 5.2 and 3.8%, respectively. In both cases, WC, Co_3W_3C, and metallic Co were detected by x-ray diffraction. A lower carbon content corresponded to higher amounts of Co_3W_3C.

3. Experimental

3.1 Spray Powders

The suppliers, tradenames, preparation methods, and nominal particle sizes of the four commercial spray powders selected for this work are compiled in Table 1. Powders 2 and 3 represent one type of powder with a fine (powder 2) or a coarse (powder 3) particle size.

Table 1 Product information for the investigated WC-10% Co-4% Cr spray powders

Powder	Supplier	Tradename	Powder type	Nominal grain size, μm
1	Sulzer Metco	Amdry 5843	Sintered and crushed	11 to 45
2	H.C. Starck	Amperit 553.065	Sintered and crushed	10 to 30
3	H.C. Starck	Amperit 553.074	Sintered and crushed	15 to 45
4	Deloro Stellite	JetKote 7109	Agglomerated and plasma densified	10 to 53

3.2 Investigation Methods

The complete characterization of the spray powders can be divided into the characterization of the physical properties (morphology, particle size distribution, and porosity) and the determination of the chemical and phase compositions.

The morphology of the powders was investigated using a scanning electron microscope (Stereoscan 260, Leica, Bensheim, Germany). The spray powder particles were embedded in a cold-setting resin and then ground and polished for microstructural investigations. These cross sections were examined in the as-polished condition and after etching with Murakami solution. The density of the powders was measured in a helium pycnometer (Accupyc 1305, Micromeritics (Norcross, GA)). The flowability of the powders was determined according to ISO 4490. The powder particle size distribution was determined by a laser particle sizer (Mastersizer, Malvern Instruments, Malvern, Worcestershire, U.K.).

The porosity of the powders was investigated by measuring nitrogen adsorption isotherms and mercury intrusion plots with an ASAP 2010 and a Poresizer 9320 (both Micromeritics). From the nitrogen adsorption isotherms, the specific surface areas according to Brunauer, Emmett, and Teller (BET) and the pore size distributions were calculated.[29,30] For comparison and confirmation, the specific surface areas were additionally obtained from measurements in which krypton was used as the adsorptive. The use of krypton is recommended for low specific surface areas.[29,30] The mercury intrusion plots were obtained in the equilibrium measurement mode, with an equilibrium time of 20 s. The information about the inner porosity of the spray powders obtained from these two methods was compared with that obtained from low-magnification SEM micrographs of metallographically prepared cross sections of the spray-powder particles in the as-polished condition.

Metallographically prepared cross sections of spray powder particles in the as-polished condition, as well as after etching with Murakami solution, were also used to study the microstructures by SEM. In order to correlate the phases detectable in the micrographs with the results of x-ray diffraction, energy-dispersive x-ray (EDX) mapping was performed.

Cobalt, chromium, and iron (assumed to be the most important impurity) contents were analyzed by inductively coupled plasma-emission spectrometry (ICP; Horizon, Fisons) of digested samples. Oxygen and nitrogen contents were measured using a LECO TC-436 (LECO Corporation, St. Joseph, MI), and the total carbon content was measured using a LECO CS-444. The free-carbon content was determined by combustion (LECO RC-412) after all of the components except free carbon had been dissolved in a mixture of hydrofluoric and nitric acid and the resulting suspension had been filtered.

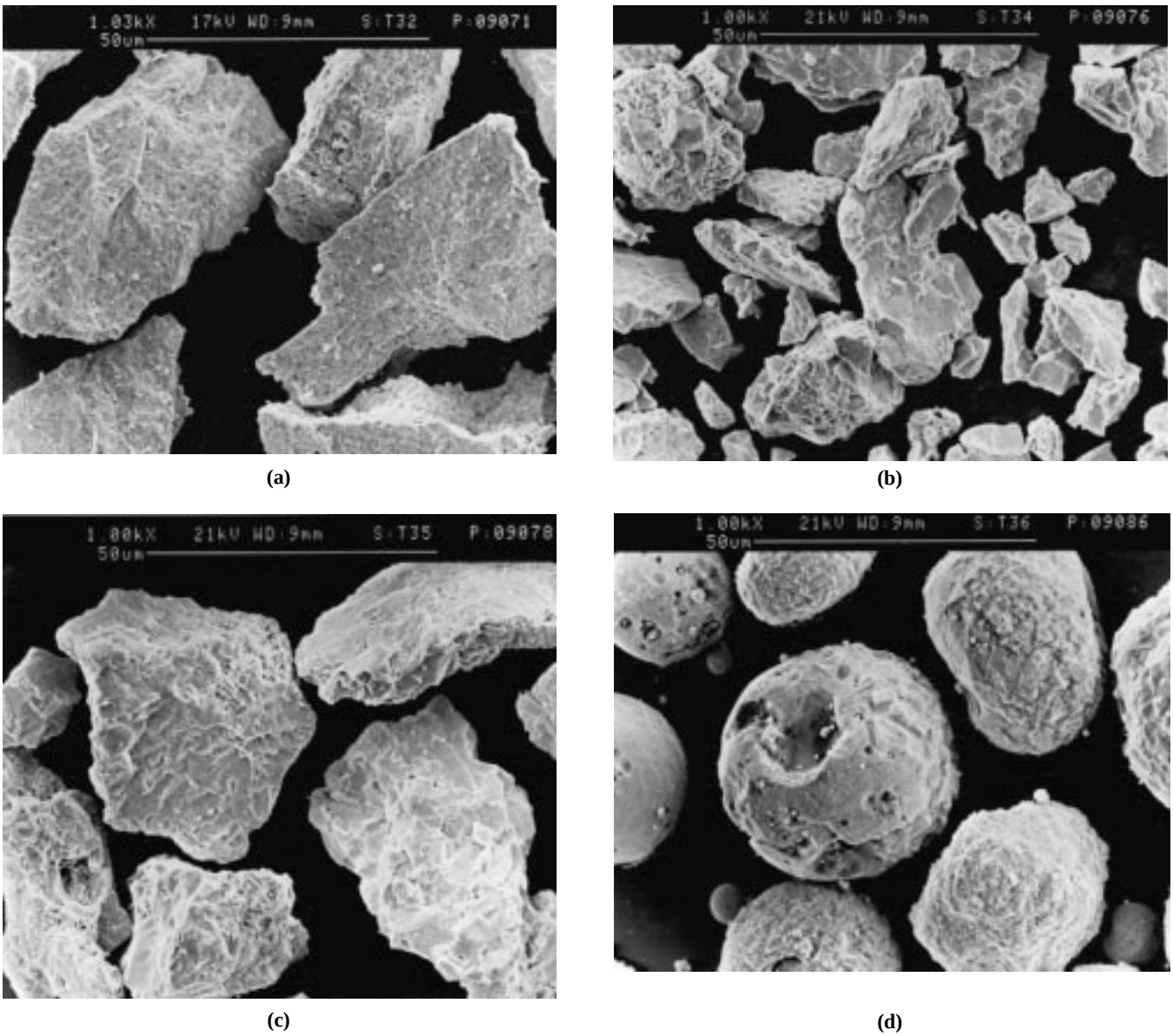

Fig. 1 SEM micrographs (secondary electron images) of (**a**) powder 1, (**b**) powder 2, (**c**) powder 3, and (**d**) powder 4

The phase composition was investigated by x-ray diffraction (XRD 7, Seifert FPM, Freiberg, Germany) using Cu K_α radiation in the range $2\theta = 15$ to 80° with a step size of 0.05° and a scanning time of 5 s. Valuable and fast information about the phase contents was also obtained by measurement of the magnetic saturation (Sigmameter, Setaram, Saint-Cloud, France).

For investigations of the influence of powder constitution on the melting of the powders, DSC measurements up to 1465 °C (DSC 404, Netzsch, Selb, Germany) were used. An argon atmosphere and a heating rate of 10 K/min were used for the measurements. Two heating and cooling cycles were investigated for each powder in order to detect thermally induced processes during the first heating cycle.

In order to check the thermal stability of the phases and deviations of the phase compositions from thermodynamic equilibrium, the spray powders 1, 2, and 4 were annealed in a carbon tube furnace (model 1000-3560-FP20, Thermal Technology Astro Division, Santa Rosa, CA) at 1000 °C for 24 h under streaming argon and cooled rapidly to room temperature in the cooling chamber of the furnace. After this treatment, the x-ray diffraction measurements and, in one case (powder 4), the chemical nonmetal analysis were repeated. Metallographic cross sections were prepared from these annealed powders and investigated by SEM in the as-polished state and after etching with Murakami solution.

4. Results

4.1 Physical Properties

Morphology. The morphology of representative powder particles is shown in the SEM micrographs in Fig. 1(a) to (d).

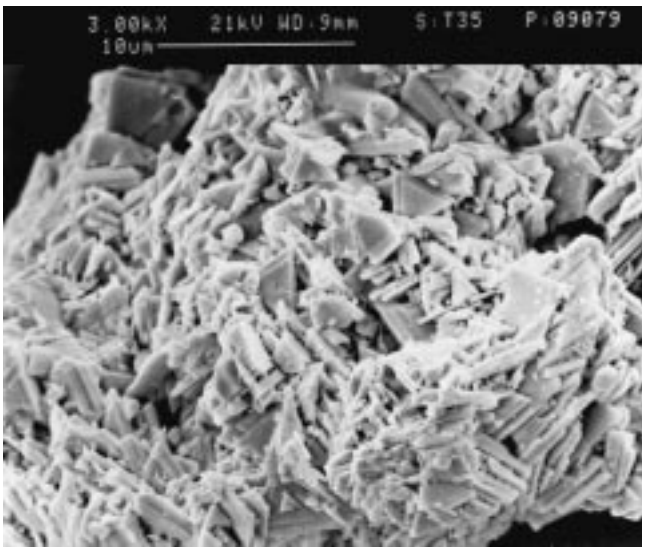

Fig. 2 SEM micrograph (secondary electron image) of a particle of powder 3, which has a deficit of binder phase

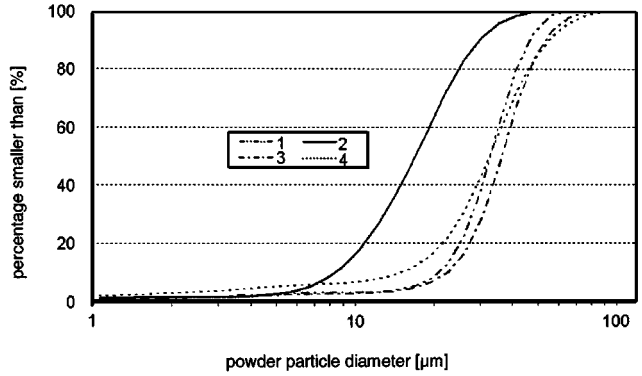

Fig. 3 Cumulative powder particle size distribution plots of powders 1 to 4

Powders 1 to 3 of the sintered-and-crushed type show typical angular and blocky shapes. At higher magnifications, the mostly dense, homogeneous surfaces, which are free of pore entrances, become even more apparent. However, there is also a significant number of spray powder particles, especially in powders 2 and 3, with a different surface appearance. An example (powder 3) is shown in Fig. 2, in which the WC crystals appear to be just loosely stuck together. As shown using other methods discussed below, this is probably caused by inhomogeneous distribution of the binder elements.

The shape of the particles of the agglomerated and plasma-densified powder 4 is nearly spherical, with smooth (binder-rich) or rough (carbide-rich) surfaces. In some particles, defects, which probably originated from the spray-drying process, and pore entrances can be observed.

Powder Particle Size Distribution. Cumulative plots of the particle size distributions of the powders are shown in Fig. 3; the amounts of particles smaller and larger than the nominal grain sizes given by the powder producers are listed in Table 2. The

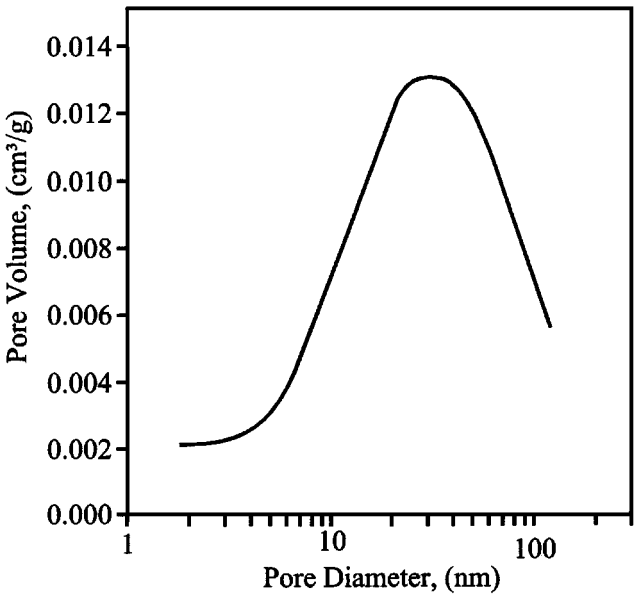

Fig. 4 Pore size distribution of powder 4 calculated from the desorption branch of the adsorption isotherm

large amount of particles with sizes above the nominal particle size of all of the powders is remarkable, as is the surprisingly large amount of fine par ticles in the plasma-densified powder 4. However, the results of particle size distribution measurements are known to be strongly influenced by the method of sample preparation. The procedure and the equipment used in this study might differ from the quality-control measurements of the suppliers.

Flowability. The flowability, also compiled in Table 2, is closely connected with the particle shape and grain size. Therefore, the plasma-densified powders were expected to exhibit good flowability. Although powder 2 was not flowable according to the conditions of this test (probably because its particle size was lower than that of powder 3), its sprayability was good, as described in Part 2 of this paper.

Density. The powder densities obtained by helium pycnometry are also compiled in Table 2. The theoretical density calculated from the densities of the nominal components of the composition WC-10% Co-4% Cr is 13.93 g/cm^3. Due to the uncertainties with respect to the densities of tungsten-containing phases present in the spray powder particles, the reliability of this value is limited. The significantly lower density of the plasma-densified powder 4 is an indication of high porosity, which was confirmed by other methods.

Porosity. The open porosity of solids can be investigated by nitrogen adsorption measurements[29,30] and mercury porosimetry,[29] which, with the available equipment, permit the identification of porosity up to pore sizes of approximately 250 nm and in the size range of 6 nm to 200 μm, respectively. With the exception of powder 4, pores detectable by nitrogen adsorption isotherms were not found. For powder 4, the pore size distribution calculated from the desorption branch of the isotherm has a maximum between 20 and 50 nm (Fig. 4). The specific surface areas, a_s, according to BET are also listed in Table 2. There is a good correlation between the specific surface areas calculated

Table 2 Data on spray powder characteristics, where a_s is the specific surface area according to BET

Powder	Particles below nominal grain size, %	Particles above nominal grain size, %	Flowability s/50 g	Density g/cm³	a_s (BET), N_2 m²/g	a_s (BET), Kr m²/g
1	2.9	30	18.9	13.7	0.11	0.14
2	10.5	17	—	14.7	0.14	0.13
3	3.0	43	14.8	14.4	0.07	0.07
4	12.0	26	13.4	11.7	0.38	0.40

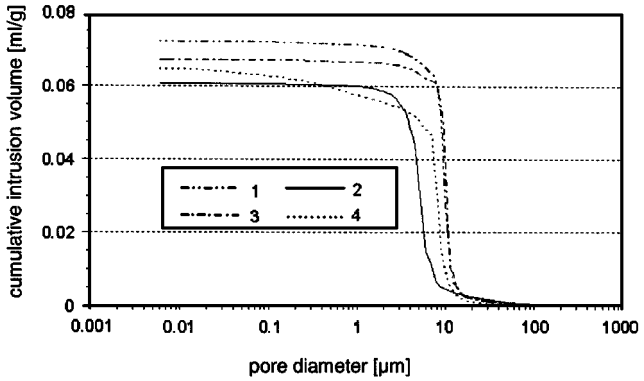

Fig. 5 Mercury-intrusion plots of powders 1 to 4

from measurements using nitrogen and krypton as the adsorptive. The relatively high values of a_s for powder 4 indicate the presence of pores that are either undetectable or hard to detect by mercury intrusion or by the investigation of cross sections with SEM. Less probably, they may also result from finely dispersed free carbon found in the powder (refer to section 4.2).

The mercury intrusion plots for powders 1 to 4 are shown in Fig. 5. The diameter of pores in a solid is directly related to the intrusion pressure according to the Washburn equation.[29] The investigation of the pore size distributions of spray powders is complicated by the fact that, at the filling pressure, the mercury is not completely intruded into the space between the individual spray powder particles. This takes place only by increasing the pressure, thus leading to a partial overlap of the intrusion into the actual pores. The pressure required for the intrusion into the space between the powder particles depends on the particle size. This is evident from the different intrusion plots of powders 2 and 3.

The high porosity of powder 4 results in a continuing intrusion at higher pressures, whereby pores with diameters in a range of approximately 20 nm to 2 μm are filled. This filling process proceeds continuously and results in the absence of a maximum in the plot of the pore size distribution. The size range of the finest pores detectable by mercury intrusion and the maximum in the pore size distribution of the adsorption measurement (Fig. 4) are in agreement.

Information on the porosity of the spray powders is also obtained from the low-magnification SEM micrographs of the as-polished powder cross sections shown in Fig. 6(a) to (c). Only a few porous particles are visible in the micrographs of all three sintered and crushed powders. In the case of powder 1, it is difficult to distinguish between pores and the cobalt binder, which appears dark in the cross sections. There is no significant difference between powders 2 and 3; for this reason, only the micrograph of powder 3 is shown in Fig. 6(b). Large spherical pores are a characteristic feature of powder 4, as can be observed in Fig. 6(c).

4.2 Chemical and Phase Composition

Chemical Composition. The results of the chemical analyses are compiled in Table 3. The differences between powders 2 and 3 are negligible, confirming that they can be treated as identical from the point of view of chemical composition. For all of the powders, the contents of cobalt and chromium found are close to the nominal contents. Major differences were detected for the bonded carbon content, which is calculated as the difference between the measured total and free-carbon contents. For all of the powders, a significant deficiency in bonded carbon compared to the nominal content of 5.27% was found. At the same time, a relatively large amount of free carbon was detected in powder 4. Simultaneously, powder 4 is characterized by the highest oxygen content. The amount of iron is more significant for the sintered and crushed powders and is obviously a result of the intensive comminution operations carried out during production of the powders.

Measurement of the Specific Magnetic Saturation. The measurement of the specific magnetic saturation is a fast and reliable standard method of quality control, which is widely used in the hardmetal industry.[31] With this method, the amount of ferromagnetic phases in the composite can easily be detected. The formation of solid solutions of cobalt with tungsten, as well as the formation of η-phases, results in a decrease in the magnetic saturation. The value for the magnetic saturation of pure cobalt is 202 μTm³/kg. Alloying elements in solid solution in the cobalt binder such as chromium and tungsten decrease the specific magnetic saturation. A content of 4% Cr lowers this value to 173 μTm³/kg, about 86% of the value for pure cobalt.[32] The values measured for the spray powders and those calculated for the binder are compiled in Table 4. The very low values for the specific magnetic saturation of powders 2 and 3 indicate that only a minor amount of the cobalt might still persist as a metallic binder alloy.

Phase Analysis by X-Ray Diffraction. The results of the x-ray diffraction measurements are also summarized in Table 4. In all spray powders, WC (JCPDS card 25-1047) was identified as the main phase.

In powder 1, in addition to WC, the η-phase Co_3W_3C (JCPDS card 27-1125) was identified, with diffraction lines shifted to lower lattice parameters (which is, as shown below, caused by the presence of chromium in its crystal lattice), together with

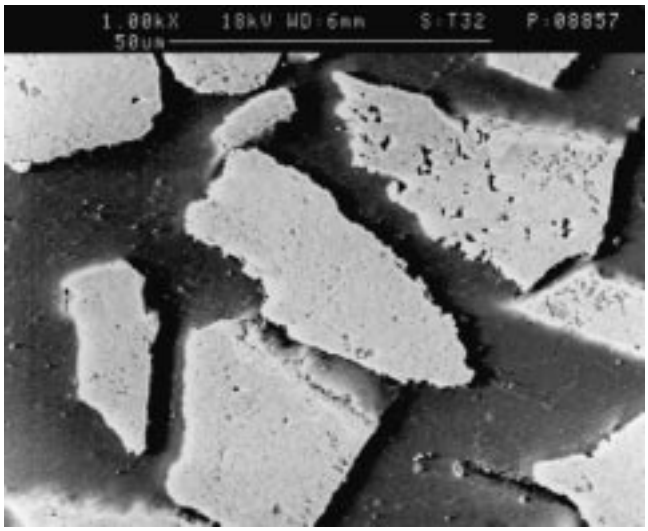

(a)

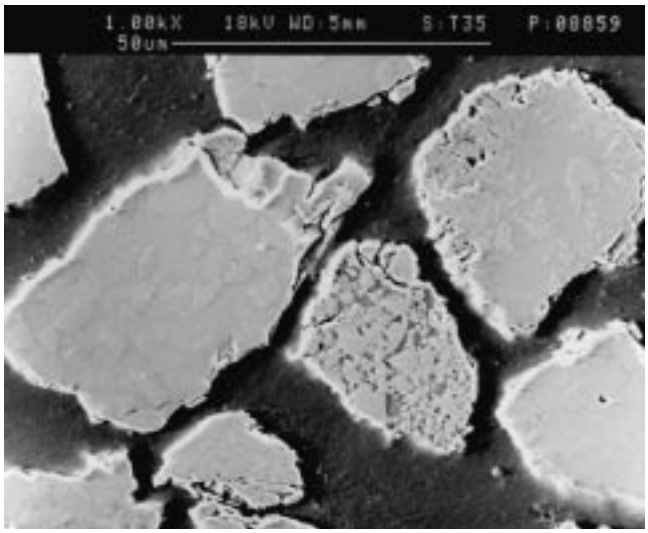

(b)

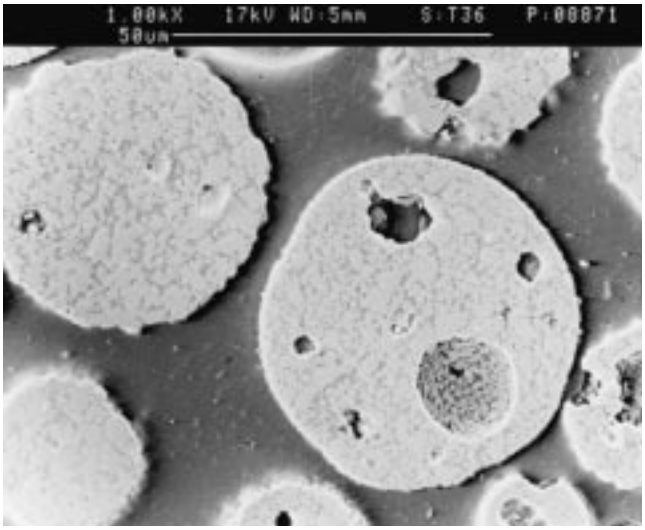

(c)

Fig. 6 SEM micrographs (secondary electron images) of the cross sections of (**a**) powder 1, (**b**) powder 3, and (**c**) powder 4

Table 3 Results of chemical analysis (mass%) of the spray powders, including powder 4 after heat treatment at 1000 °C

Powder	%Co	%Cr	%Fe	$\%C_{total}$	$\%C_{free}$	$\%C_{bond}$	%O	%N
1	10.5	4.1	0.37	5.10	0.17	4.93	0.06	<0.01
2	10.5	3.9	0.14	3.56	<0.01	3.55	0.05	0.01
3	10.7	3.8	0.17	3.65	0.01	3.64	0.03	0.01
4	10.3	3.3	0.07	5.15	0.61	4.54	0.15	0.01
4, 1000 °C	…	…	…	5.15	0.07	5.08	0.02	0.01

metallic cobalt (JCPDS card 15-806) with a somewhat higher lattice parameter, probably due to alloy formation with chromium and tungsten.

It was confirmed that powders 2 and 3 are also identical with respect to their phase composition. The positions of the lines of Co_3W_3C in these powders correspond to those given in the standard (JCPDS card 27-1125). Besides Co_3W_3C and the main phase WC, a set of lines was detected, which were originally interpreted as those of the κ-phase $Co_3W_9C_4$ (JCPDS card 6-616), but for which the agreement was poor.[2] More detailed investigations and calculations showed that the composition of this phase should rather be described by the formula $Co_6Cr_2W_{18}C_7$. The diffraction lines for metallic cobalt were not found.

In powder 4, a set of diffraction lines of W_2C shifted to smaller lattice parameters compared to those of the pure phase (JCPDS card 35-776) was detected.[2] This shift can be explained by the replacement of a fraction of the tungsten atoms in W_2C by chromium. The calculated lattice parameters of $a = 0.297$ nm and $c = 0.471$ nm indicate a replacement of approximately 10 to 15 mol.% of W_2C by "Cr_2C," according to Stecher *et al.*[11] However, there is also good agreement with the range containing 30 to 45 mol.% "Cr_2C" in $(W, Cr)_2C$ having a constant lattice parameter, according to Eremenko *et al.*[12] Caused by the high cooling rate during powder preparation, probably a tungsten- and chromium-rich cobalt binder solidifies from the melt, besides WC and $(W, Cr)_2C$. This is indicated by the shift of the diffraction lines toward somewhat higher lattice parameters, which is probably caused by the presence of a W-rich supersaturated Co-W-Cr-alloy.

Phase Identification in the Cross Sections. The low-magnification SEM micrographs in Fig. 6(a) to (c) show that, in powders 1 and 4, all particles have quite similar microstructures, whereas in powder 3 (Fig. 6b) (as well as in powder 2), particles with different microstructures exist and the distribution of the elements and the phases appears to be inhomogeneous. In one of the particle types, bright WC particles are embedded in a gray matrix; in another type, they are embedded in a dark matrix. The number of particles where WC grains are embedded in a gray matrix is higher. For better identification of the phases present and evaluation of the WC grain size, higher magnifications were used. The cross sections of the most characteristic particles in the as-polished state are shown in Fig. 7(a) (powder 1), 7(b) and (c) (different types of particles of powder 3), and 7(d) (powder 4).

The grain size of WC, which appears bright in all powders as shown below, differs greatly between the powders. It is the lowest in powder 1 (less than 3 μm), average in powder 4 (approximately 3 to 5 μm), and largest in powders 2 and 3. In addition,

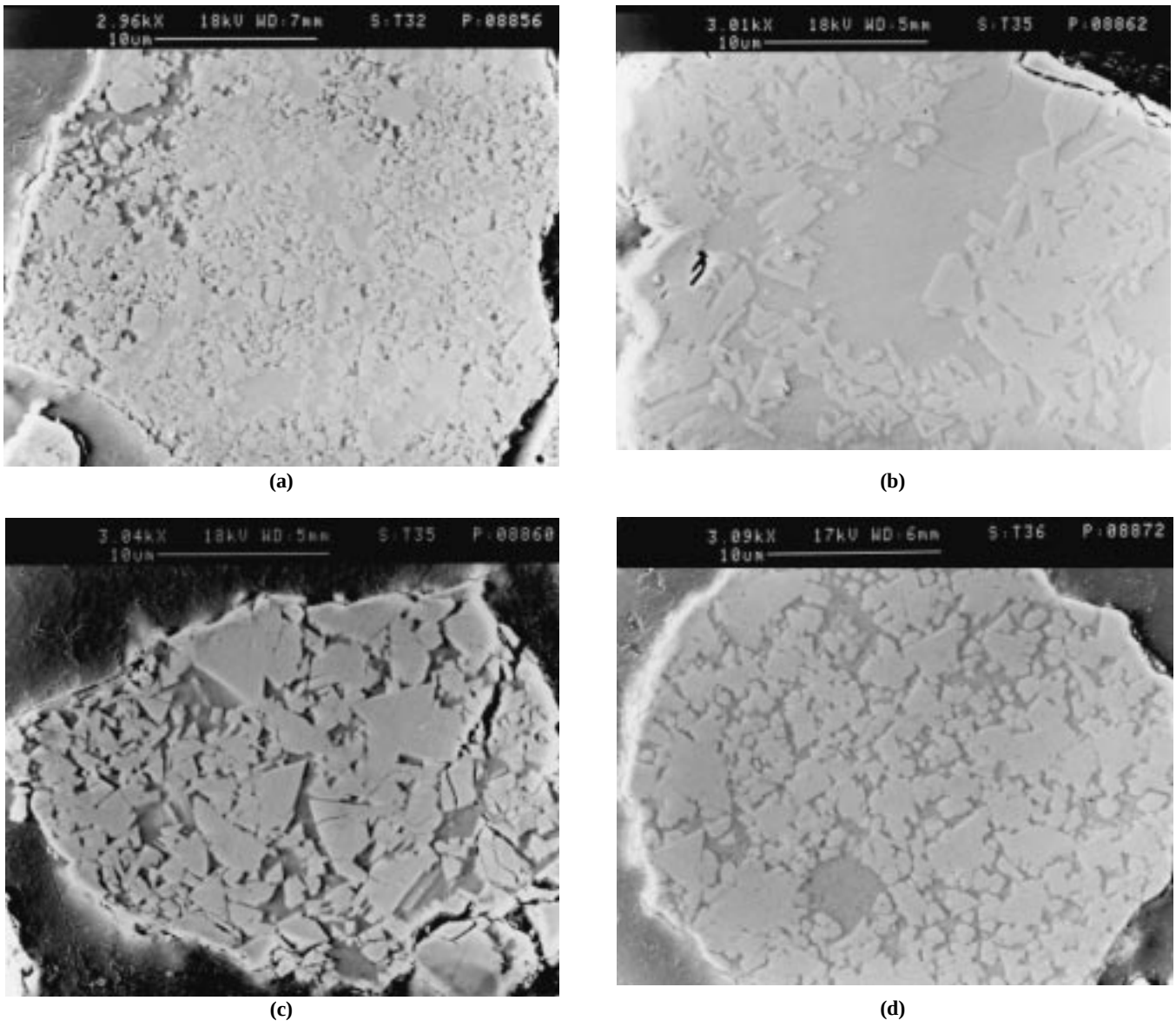

Fig. 7 High-magnification SEM micrographs (secondary electron images) of the cross sections of individual particles of (**a**) powder 1, (**b**) and (**c**) powder 3, and (**d**) powder 4

Table 4 Values of the magnetic saturation and phases detected by x-ray diffraction (the asterisk indicates lines shifted compared to the standard)

Powder	Magnetic saturation (measured) $\mu Tm^3/kg$	Magnetic Saturation of the binder (calculated) $\mu Tm^3/kg$	Main phases	Medium phases	Minor phases
1	8.8	83.8	WC	…	Co_3W_3C*, Co*
2	0.4	3.8	WC	Co_3W_3C, $Co_6Cr_2W_{18}C_7$	…
3	0.6	5.6	WC	Co_3W_3C, $Co_6Cr_2W_{18}C_7$	…
4	6.7	65.0	WC	$(W,Cr)_2C$	Co*

the distribution of the WC grains in powders 2 and 3 is very inhomogeneous, some particles with the gray binder matrix containing only a small amount of WC grains.

More details on the distribution of the elements and phases are revealed by the results of EDX mapping of individual spray powder particles, shown in Fig. 8(a) (powder 1), (b) and (c) (different particles of powder 3), and (d) (powder 4). In each of the figures, a secondary electron image and elemental maps of tungsten, cobalt, and chromium are shown for one area.

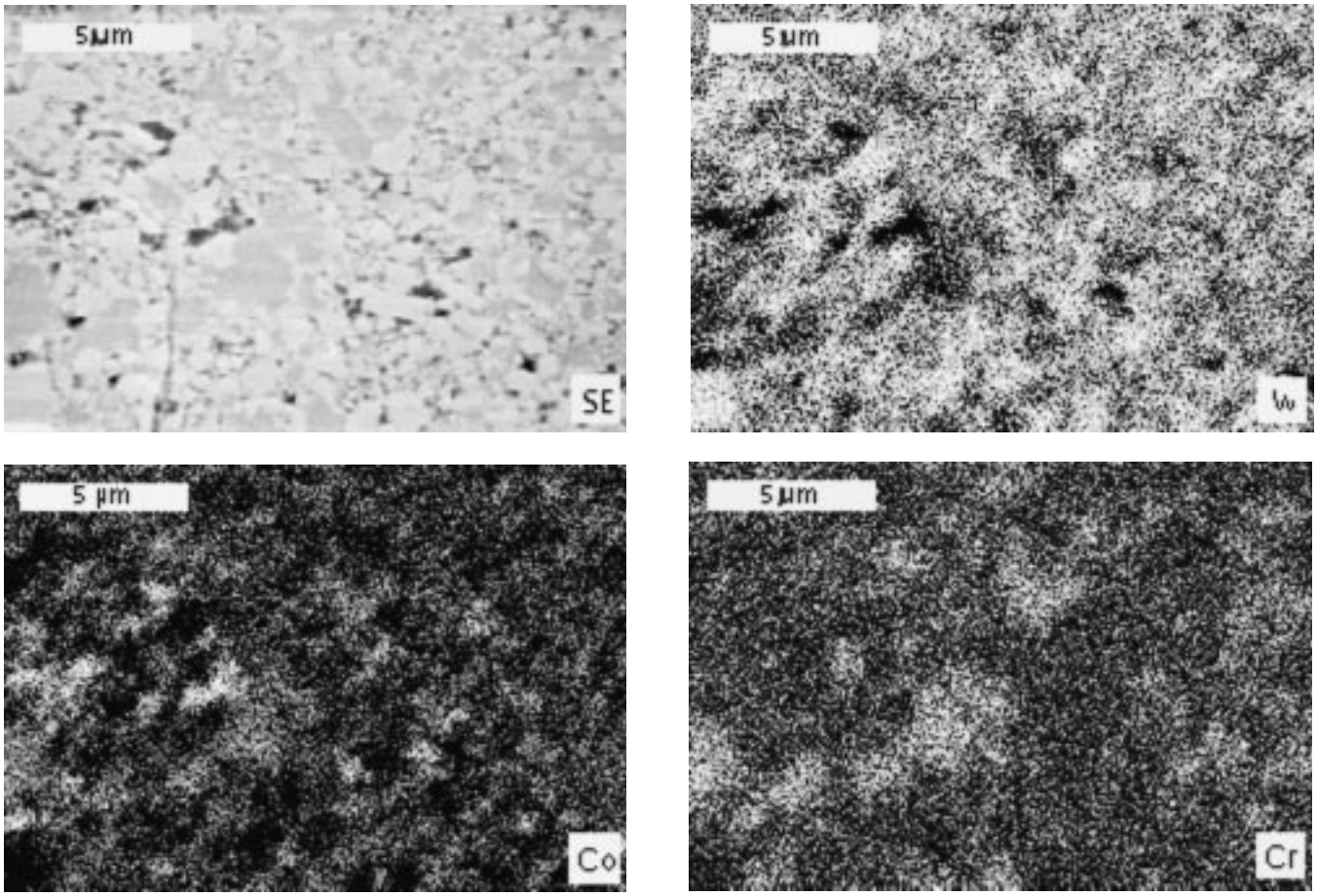

(a)

Fig. 8 EDX mappings (secondary electron image, tungsten, cobalt, and chromium elemental maps) of individual particles of (**a**) powder 1, (**b**) and (**c**) powder 3, and (**d**) powder 4 (continued on next page)

In powder 1 (Fig. 8a), the small bright areas correspond to WC and the small dark areas correspond to the cobalt binder alloyed with chromium. The larger gray areas contain all three metallic elements, and, according to the results of x-ray diffraction, can be correlated with the η-phase. Most of the chromium present in the composite is concentrated in these areas.

The EDX mapping of a representative particle of powder 3 with bright grains and larger gray areas (Fig. 8b) shows the existence of not two but three phases. The bright grains can be clearly identified as WC. Elemental mapping of these grains shows no presence of Co and only a small amount of Cr. The area appearing gray in the SE image contains all three metallic elements W, Co, and Cr. The content of Cr is nearly the same over the entire gray area, while the area in the upper left corner is richer in W and poorer in Co. To the left of the WC grain in the lower right area, a pullout caused by the metallographic preparation is present. The area in the upper left corner can be designated as the κ-phase with the composition $Co_6Cr_2W_{18}C_7$, while the bright WC particles are embedded in the η-phase $(Co, Cr)_3W_3C$.

The EDX mapping of a particle with bright angular grains and dark intergranular areas, which are in the minority but still present in a significant amount, is shown in Fig. 8(c). It reconfirms that the bright grains consist of WC and that no cobalt or chromium is present in these grains. Both cobalt and chromium are distributed between these grains, but they appear rather more separated than mixed. Since cobalt and chromium form extensive solid solutions, it is improbable that the cobalt and chromium metals can coexist without forming alloys. It is more probable that a chromium-rich carbide such as $(Cr, Co, W)_7C_3$, which has locally formed, exists together with some metallic cobalt. However, the gross amounts of these phases in the spray powder are so low that such phases cannot be detected by x-ray diffraction. It can be assumed that the maximum sintering temperature of these particles was lower than those shown in Fig. 8(b). It should be mentioned that, because of the inhomogeneous distribution of the elements, spray powder particles with yet other microstructures can occasionally be detected.

Finally, Fig. 8(d) shows the EDX mapping of a particle of powder 4. Again, the bright grains, which have a rounded shape in this powder, consist of WC. Cobalt and chromium are distributed around these grains. However, cobalt is concentrated, whereas chromium is more diffuse, appearing to be present in the outer rim of the WC grains as well as around them. It is known that, in thermally sprayed coatings (the process of plasma

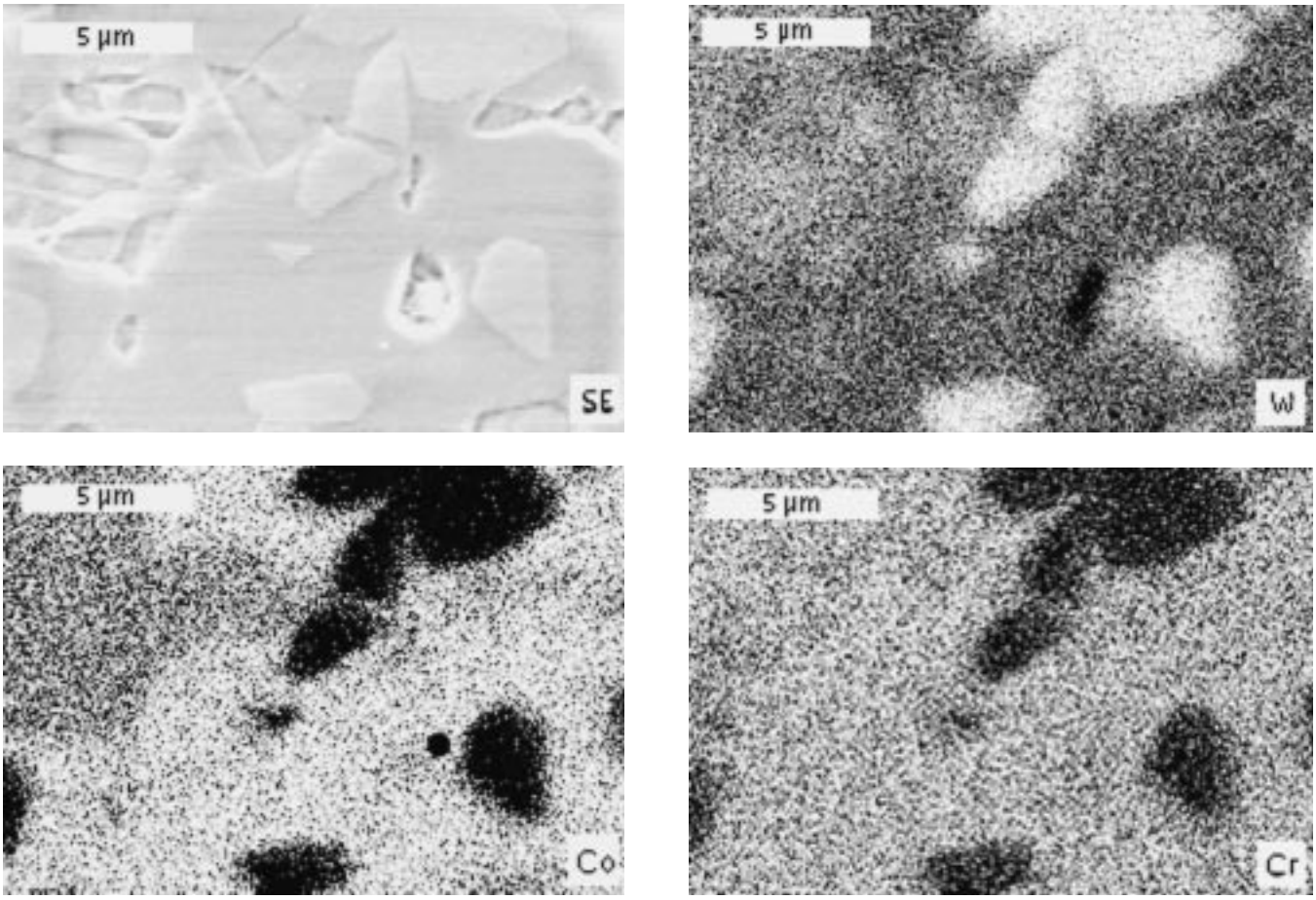

(b)

Fig. 8 (continued) EDX mappings (secondary electron image, tungsten, cobalt, and chromium elemental maps) of individual particles of (**a**) powder 1, (**b**) and (**c**) powder 3, and (**d**) powder 4

densification has to be regarded as being similar), WC grains are often found to be surrounded by rims of W_2C.[4,33,34] This phase easily incorporates chromium in the lattice forming $(W, Cr)_2C$, which is detected by x-ray diffraction.

Thermal Analysis. Figure 9(a) to (c) show the DSC plots of a first (solid line) and a second (dashed line) heating run for powders 1, 2, and 4. For all powders, the shift in the baselines of the first and second heating run is caused by the sintering of the material during the first heating run and the resulting change in thermal conductivity. The plots of the cooling cycles for the first and second heating run coincide in all cases.

For powders 1 and 4, sharp peaks of an endothermic effect connected with the formation of the melt were detected. For the first heating run, the onset temperatures were determined to be 1212 °C (powder 1) and 1220 °C (powder 4). The corresponding maximum temperatures were found to be 1222 °C and 1226 °C for powders 1 and 4, respectively. In the case of powder 4, it appears that the endothermic melting of the binder phase has interrupted an exothermic reaction. It can be speculated that this is caused, for instance, by the reaction of $(W, Cr)_2C$ with cobalt, leading, as shown below, to the formation of the η-phase. In contrast to powders 1 and 4, the DSC plot of powder 2 up to 1465 °C gives no indication of a melting reaction.

The exothermic effect of resolidification during cooling both for powders 1 and 4 is subdivided into two peaks, as shown for powder 1 in Fig. 10. For the first cycle, the maximum temperatures of the first and second peaks were 1210 °C and 1200 °C for powder 1 and 1222 °C and 1206 °C for powder 4.

4.3 Results of the Heat Treatment

The phase constituents of the powders as identified by x-ray diffraction after heat treatment at 1000 °C of powders 1, 2, and 4 are summarized in Table 5.

The phase composition of powder 1 is close to that in thermodynamic equilibrium. Therefore, it was expected that the heat treatment of this powder does not cause any changes. No mass loss was detected as a result of the heat treatment and the phase composition was unchanged. Only small, nearly negligible shifts in the positions of the diffraction lines of the η-phase and the alloyed cobalt binder were observed. In SEM investigations of the cross section, the microstructure of the spray-powder particles was found to be similar to that of the original powder.

A small mass loss of 0.03% was found as a result of the heat treatment of powder 2. Only the lines of WC and the η-phase of the type M_6C were detected. The lines of the modified κ-phase

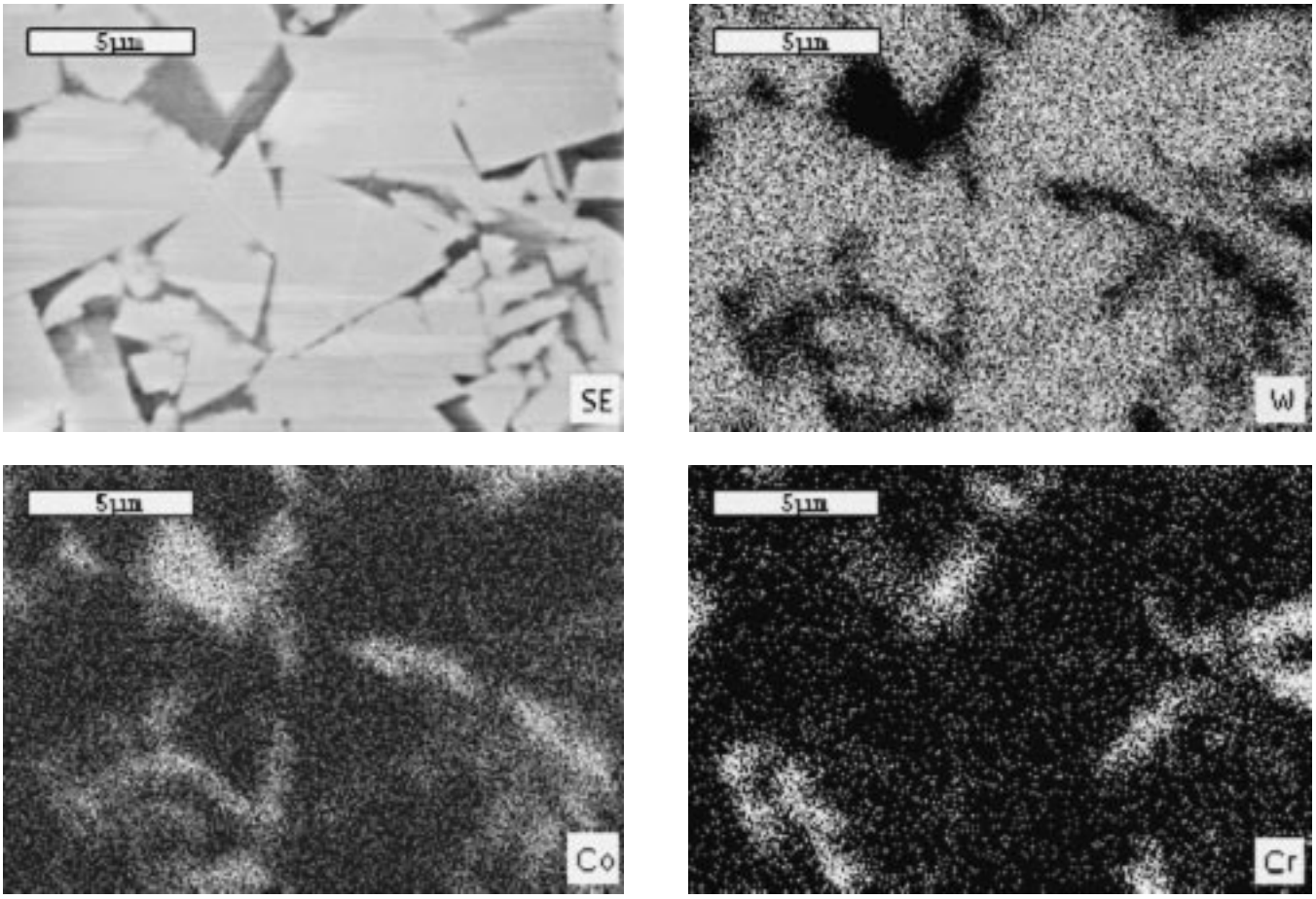

(c)

Fig. 8 (continued) EDX mappings (secondary electron image, tungsten, cobalt, and chromium elemental maps) of individual particles of (**a**) powder 1, (**b**) and (**c**) powder 3, and (**d**) powder 4

$Co_6Cr_2W_{18}C_7$ disappeared, confirming that the phase composition of the original powder was not in thermodynamic equilibrium. Assuming that only WC and the η-phase are present in the heat-treated spray powder, from the gross chemical composition, the composition of the η-phase can be calculated as $(W_{2.78}Cr_{0.92}Co_{2.3})$ C. Remarkably, no change in the position of the diffraction lines of the η-phase as a result of the heat treatment was found. In both cases, the position of the lines agrees with the standard (JCPDS card 27-1125). Furthermore, no change in the microstructure was found by SEM investigations of the cross sections. No thermal effect connected with the decomposition of $Co_6Cr_2W_{18}C_7$ was detected by DSC, which might be due to the relatively low amount of $Co_6Cr_2W_{18}C_7$ in the starting powder and/or the low thermal effect of this reaction.

As a result of the heat treatment, a mass loss of 0.2% was found for powder 4. The oxygen content was lower than that of the as-received powder, indicating that a reduction process occurred. However, the total carbon content was found to be unchanged. More important is the fact that, after the heat treatment, the carbon is now nearly completely bonded in other phases and free carbon is present only in a low amount. In the x-ray diffraction pattern, instead of $(W, Cr)_2C$, the lines of the η-phase M_6C shifted to lower lattice parameters were detected. This behavior was expected since $(W, Cr)_2C$ in the original spray powder is not in thermal equilibrium with the metallic binder. The lines of the cobalt binder are shifted toward a higher lattice parameter, but less than in the original spray powder (the position of the strongest peak shifts from 2θ = 43.05 to 43.76°). Only in the case of powder 4 was significant information obtained from SEM micrographs after etching. The SEM micrographs of etched cross sections in the as-received state and after the heat treatment are shown in Fig. 11(a) and (b), respectively. Originally,[2] the etched areas were interpreted as the η-phase and not as $(W, Cr)_2C$. However, the η-phase appearing in the powder after the heat treatment is etched by the Murakami solution in a different way, as can be seen in Fig. 11(b).

5. Discussion

5.1 Characteristics of the Spray Powders

Powder 1 is a relatively dense powder with a typical morphology of a "sintered and crushed" powder. The carbon content and the contents of binder elements are the closest to the nominal values, and the distribution of all elements seems also to be

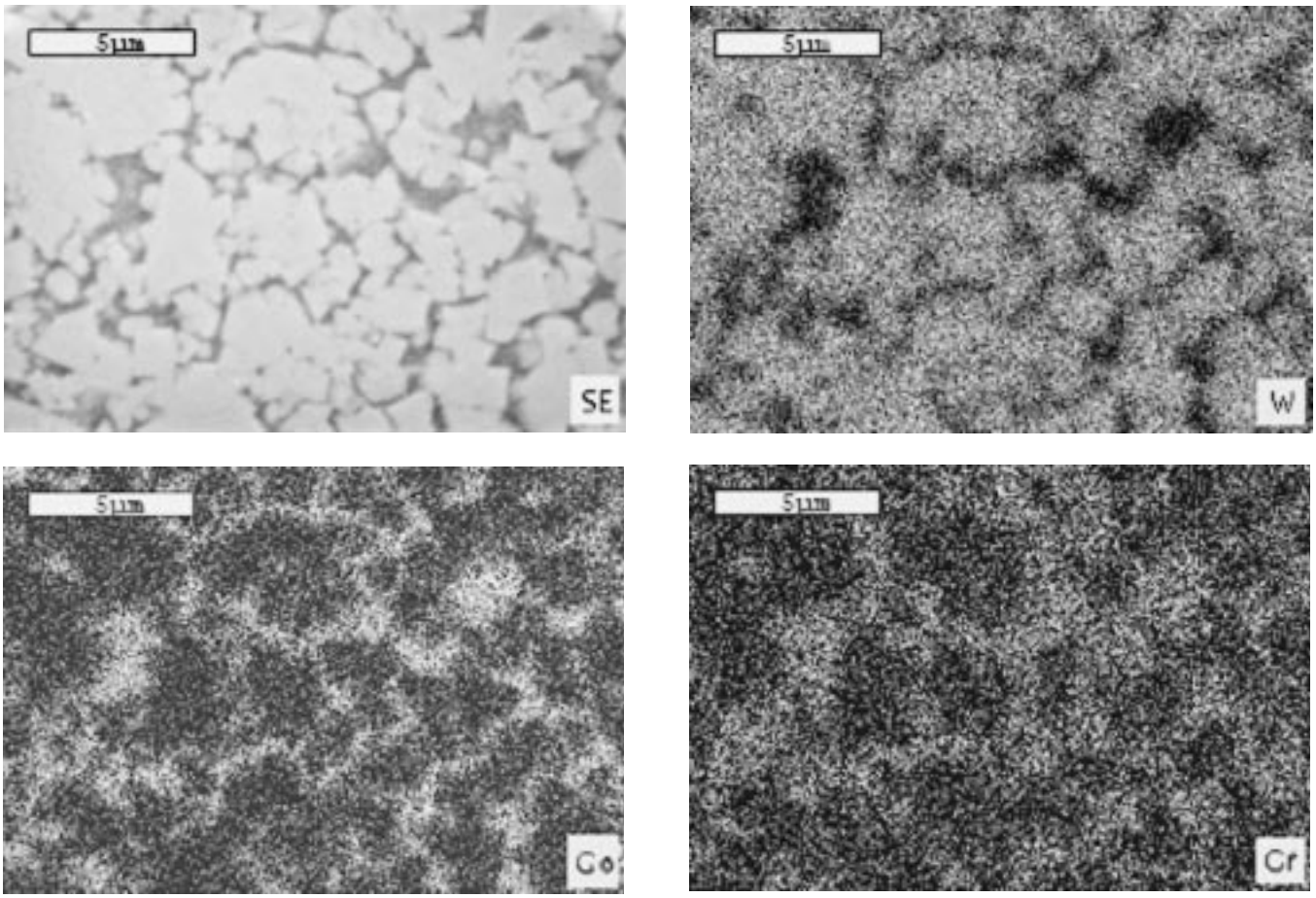

(d)

Fig. 8 (continued) EDX mappings (secondary electron image, tungsten, cobalt, and chromium elemental maps) of individual particles of (**a**) powder 1, (**b**) and (**c**) powder 3, and (**d**) powder 4

the most homogeneous of all powders investigated in this work. The presence of the phases WC, $(Co, Cr)_3W_3C$, and an alloyed cobalt binder is indicative of the thermodynamic equilibrium and presumably a result of a relatively slow cooling rate from the sintering temperature in the production process.

Powders 2 and 3, also having the typical morphologies of sintered and crushed powders, differ only in their particle size distributions, but are fully identical with respect to their chemical and phase compositions. The distribution of the elements is inhomogeneous, with two types of particles with different microstructures dominating. The carbon content is low, leading to the formation of significant amounts of η- and κ-phases. The existence of the κ-phase with the composition $Co_6Cr_2W_{18}C_7$, which is not thermodynamically stable for the given composition, as was shown by the heat treatment of the powder at 1000 °C, has led to the conclusion that the production process for this powder includes a rapid cooling process. The κ-phase is believed to be formed after primary crystallization of WC but before the η-phase is formed. Due to the carbon deficiency, the metallic binder content in the powder is extremely low. Only magnetic saturation and EDX mapping of one of the spray powder particle types indicate that some minor amounts of metallic cobalt still exist and are not bonded in carbide phases. The DSC investigations gave no indications that a melt is formed up to 1465 °C.

Powder 4 was produced by a different technology: agglomeration and plasma densification. The spherical morphology and the generally smooth surfaces of the spray powder particles result in excellent flowability. The number of particles with sizes smaller than the nominal grain size surprisingly was found to be significantly higher than in the other powders. A large number of spherical pores are contained within the spray powder particles. The origin of the pores can be attributed to spray-drying defects, which cannot be eliminated by plasma densification. Particles free of spray-drying defects are dense and show a homogeneous distribution of the elements. The process of plasma densification, which includes a high cooling rate of the material, already leads to the peritectic decomposition of WC, as indicated by the presence of free carbon and $(W, Cr)_2C$. The latter is probably formed by the reaction of the primary decomposition product W_2C with the chromium-containing liquid Co-Cr-W-C phase. The information on the distribution of the $(W, Cr)_2C$ phase in the original powder obtained by EDX mapping (around the WC grains, Fig. 8d) and from the SEM micrographs after etching (Fig. 11a) still has some ambiguities. The heat treatment at 1000 °C leads to the formation of $(Co, Cr)_3W_3C$ as the equilibrium phase of the given chemical composition.

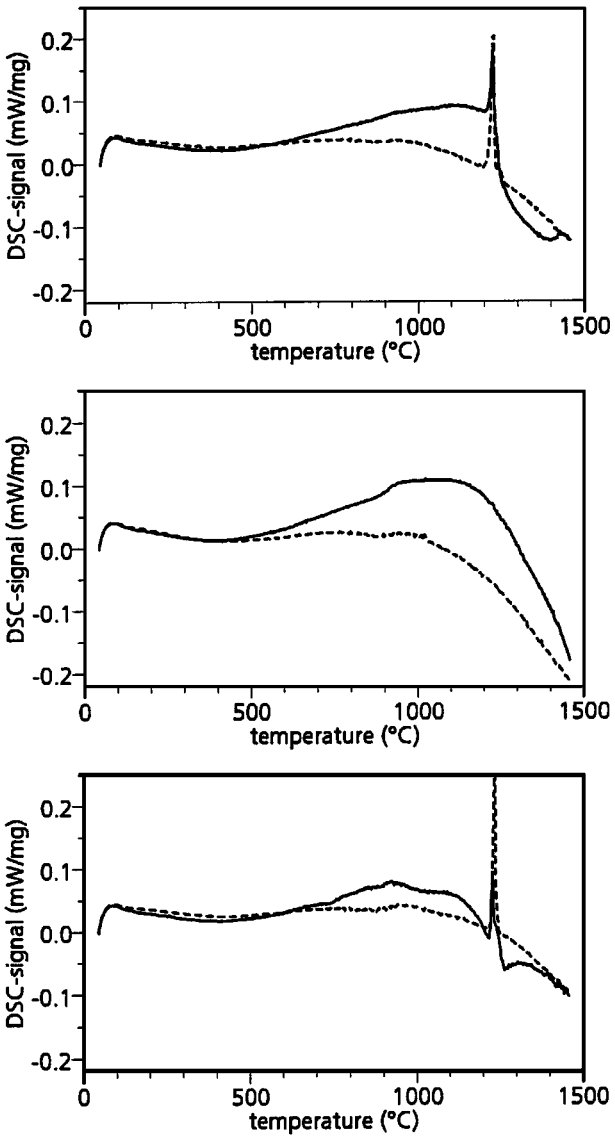

Fig. 9 DSC plots of heating stage for powders 1 (above), 2 (middle), and 4 (below). First heating: solid line, and second heating: dashed line

5.2 Comparison of the Phase Analysis with Results of Fundamental Hardmetal Research

The results of fundamental hardmetal research indicate that only part of the chromium contained in the composition of WC-10% Co-4% Cr can be dissolved in the metallic binder matrix. Therefore, this addition of chromium will lead to the formation of additional carbide phases. Which of them is formed in thermodynamic equilibrium depends on the carbon content of the hardmetal. Due to the addition of chromium as a carbide, the content of carbon in model alloys having a content of approximately 4% Cr, described by Suzuki and Tokomotu[19] or by Zackrisson *et al.*,[20] is higher than in WC-10% Co-4% Cr spray powders. For this reason, when equilibrium or near-equilibrium conditions are reached, the η-phase of the M_6C-type $(Co, Cr)_3W_3C$ was detected instead of the carbide $(Cr, Co, W)_7C_3$

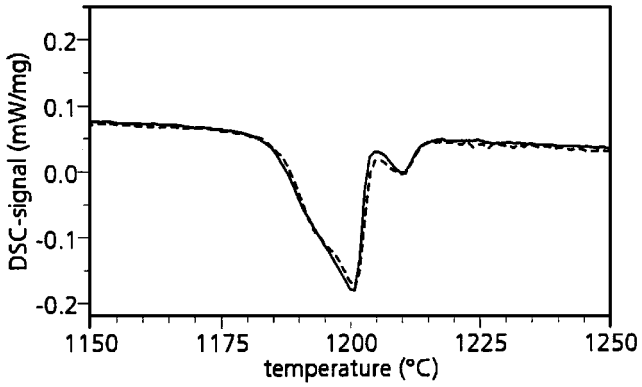

Fig. 10 DSC plot of cooling stage for powder 1 (first cooling: solid line, and second cooling: dashed line)

Table 5 Phase composition determined by x-ray diffraction of the spray powders after heat treatment at 1000 °C (the asterisk indicates lines shifted compared to the standard)

Powder	Main phases	Medium phases	Minor phases
1	WC	…	Co_3W_3C*, Co*
2	WC	Co_3W_3C	…
4	WC	Co_3W_3C*	Co*

in all spray powders. It is remarkable that the η-phase in the different spray powders probably has different compositions, evidenced by the variations shown in the lattice parameters. However, no information about how the simultaneous presence of tungsten, cobalt, and chromium affects the lattice parameter of the η-phase is available in the literature. The investigations performed in this work have also revealed that, in accordance with the literature, the phase WC does not form solid solutions with other elements, except to a very minor extent with chromium, as revealed by EDX mapping and described by Ref 12.

In addition, nonequilibrium carbide phases and products of thermal decomposition can be detected in the spray powders, probably as a result of high cooling rates in the spray powder production process and high process temperatures in the plasma-densification process. The appearance of the κ-phase in powders 2 and 3 is favored by the low carbon content. Thermal decomposition of WC during the plasma densification of powder 4 results in the formation of free carbon and W_2C. This decomposition reaction resulting in an increasing free-carbon content with increasing plasma power is also reported for APS spraying of WC-Co.[35] W_2C reacts with the chromium-containing melt and forms $(W, Cr)_2C$. At subsolidus temperatures, this phase is not in thermodynamic equilibrium with the other phases WC, C, and Co. Information on the composition of $(W, Cr)_2C$ in the literature[11,12,13] is somewhat at variance, and still less is known about its stability in hardmetal compositions and its properties. This phase is also found in a WC-20% "Cr_3C_2"-6% Ni spray powder.[36] In this other type of powder, the stability of $(W, Cr)_2C$ might be higher, due to the higher chromium content in the spray powder and the different binder metal.

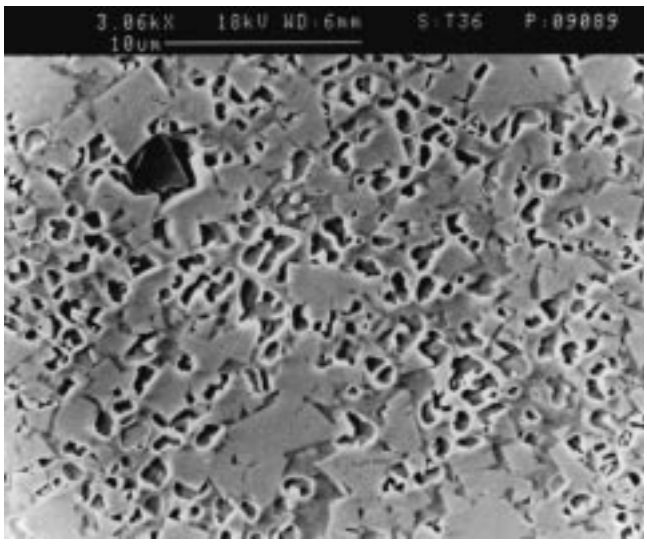

(a)

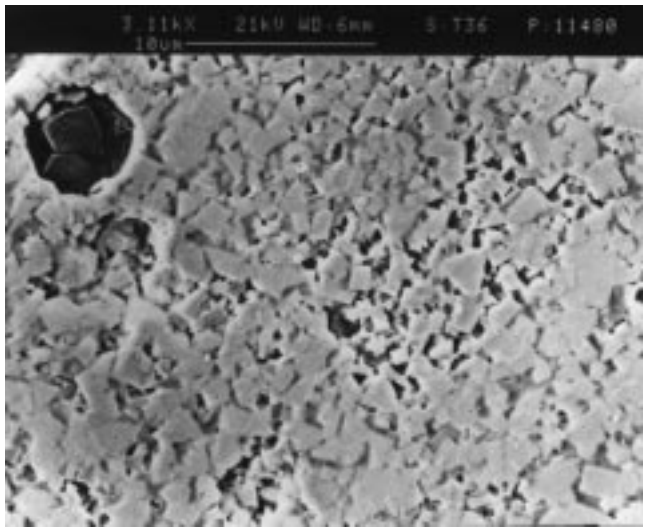

(b)

Fig. 11 SEM micrographs of the cross section of powder 4 etched with Murakami solution: (**a**) as-received and (**b**) after heat treatment at 1000 °C (Fig. 11b)

Other carbide phases, for instance, with the $M_{23}C_6$ structure, were not found in the selected spray powders.

As described above, only part of the chromium content can be retained in the binder alloy and additional carbide phases are formed. Some of the carbide phases, particularly the η-phase, do incorporate cobalt into their crystal lattices, thereby lowering the amount of the corrosion-sensitive binder phase. This effect appears to be more pronounced in the case of carbon deficiency. A general increase in the hardness and corrosion resistance, but also an increase in the brittleness, can be expected. From the early history of hardmetals, it is known that sintered corrosion-resistant wear parts consisting mostly of the η-phase have been produced under the tradename "Elmarid."[9] However, a complete disappearance of the binder phase decreases the processability in the spray process. The composition WC-10% Co-4% Cr seems to be a good empirically found formulation that is well balanced between the contradictory requirements for the preparation of simultaneous wear- and corrosion-resistant coatings. It should also be kept in mind that the chromium additions also influence the grain growth behavior of WC in the composite in all stages of the technology, ranging from the production of the spray powder to the preparation of the coating.

5.3 Comparison with Spray Powder Analyses in the Literature

The commercial powder Amdry 5843 (powder 1 in this work) has been characterized several times over the last few years.[3,7,28] The powder with the same composition and high carbon content characterized by Schwetzke and Kreye[4] can also be assumed to be identical, at least regarding its chemical and phase compositions. The good agreement of the experimental results in all works, *e.g.*, between the microstructures in the SEM micrographs of the cross sections and the x-ray diffraction patterns, should be underlined. However, there is some disagreement in the interpretation of the phases appearing in the powder with some of those works.[3,7,28] The existence of $Cr_{23}C_6$[28] or Cr_7C_3[3,7] in this composition with known carbon and chromium contents can quite safely be excluded on the basis of the information in the hardmetal literature.[19] The x-ray diffraction line appearing at $2\theta = 44.1°$ using Cu K_α radiation[3,28] can clearly be designated as the alloyed cobalt binder. The position of this line for pure cobalt (which is also the 100% peak) is 44.22°; for powder 1 in the present study, the position $2\theta = 43.95°$ was observed.

Taking into account the grain size, the characteristics of the powder with the low carbon content characterized by Schwetzke and Kreye[4] are identical to those of powder 3 (Amperit 553.074) in this work. As described above, due to the low carbon content, practically no metallic phase is present in this powder; this has a negative influence on the processability. Indeed, a low deposition efficiency (38% compared to 56% for the sintered and crushed powder with a high carbon content) is reported.[4] A lower grain size for such a powder composition (*e.g.*, powder 2, Amperit 553.065) is advantageous for effective heating of the particles in the spray process and, consequently, for better coating properties.[2]

As a result of the additional investigation methods used, several corrections and improvements in the interpretations made in our first report[2] on the powder characteristics were possible: the originally detected W_2C with shifted lines was found to be a $(W, Cr)_2C$ solid solution, which, along with the η-phase, is etched by Murakami solution. The composition of the κ-phase was calculated to be $Co_6Cr_2W_{18}C_7$. Finally, the nonequilibrium character of different phases in powders 2, 3, and 4 was shown by the heat treatment at 1000 °C.

6. Conclusions

A broad variety of physical, physicochemical, chemical, and other methods as applied in this work is necessary for a complete characterization of the microstructure and the chemical and phase compositions of WC-10% Co-4% Cr spray powders. All parameters and properties are strongly interconnected, *i.e.*, the chemical and the phase compositions, and the production tech-

nique with the morphology and the presence of different phase constituents.

The addition of chromium to WC-Co to increase the corrosion resistance of the binder causes the number of possible metallurgical reactions occurring in the material as well as the number of phases and solid solutions present to increase and makes the material even more complex. An exceptional increase in the corrosion resistance of the binder in the composition WC-10% Co-4% Cr cannot be achieved because only part of the chromium content can be retained in the cobalt binder alloy. The carbon content and the cooling rate in the spray-powder production process (leading to the formation of equilibrium or non-equilibrium hard phases) are the most important factors controlling the phase composition of the spray powder. Some of the carbide phases appearing as a result of chromium additions in excess of the solubility limit in the binder, and especially when there is a simultaneous carbon deficiency, such as the η-phase, can also incorporate cobalt into the crystal lattice, thereby lowering the amount of the corrosion-sensitive binder phase. This can have a negative effect on the sprayability of the powder. However, the composition WC-10% -4% Cr seems to be a good empirically found and balanced formulation for the preparation of simultaneous wear- and corrosion-resistant coatings.

Acknowledgments

The authors are indebted to Dr. W. Gruner (IFW, Dresden, Germany) for providing the nonmetal analyses of the spray powders and Mr. K. Jaenicke-Rößler (FhG-IKTS, Dresden, Germany) for the DSC measurements.

References

1. J. Beczkowiak, H. Keller, and G. Schwier: *Schweissen Schneiden,* 1996, vol. 48 (2), pp. 132-36 (in German).
2. L.-M. Berger, P. Vuoristo, T. Mäntylä, W. Kunert, W. Lengauer, and P. Ettmayer: in *Practical Solutions to Engineering Problems,* C. C. Berndt, ed., ASM International, Materials Park, OH, 1996, pp. 97-106.
3. J.M. Guilemany, F.J. Sánchez, L. Delaey, and L. Jacobs: in *TS'96: Vorträge und Posterbeiträge der Thermischen Spritzkonferenz '96,* E. Lugscheider, ed., Dt. Verl. für Schweißtechnik, Düsseldorf, 1996, DVS Berichte vol. 175, pp. 230-34.
4. R. Schwetzke and H. Kreye: *J. Thermal Spray Technol*., 1999, vol. 8 (3), pp. 433-39.
5. J. Berget, E. Bardal, and T. Rogne: in *Thermal Spray: A United Forum for Scientific and Technological Advances,* C.C. Berndt, ed., ASM International, Materials Park, OH, 1998, pp. 783-89.
6. J. Berget, E. Bardal, and T. Rogne: in *Thermal Spray: Meeting the Challenges of the 21st Century,* C. Coddet, ed., ASM International, Materials Park, OH, 1998, pp. 305-12.
7. L. Jacobs, M.M. Hyland, and M. De Bonte: *J. Thermal Spray Technol.,* 1998, vol. 7 (2), pp. 213-18.
8. B.R. Marple, J. Voyer, and S. Simard: in *Proc. United Thermal Spray Conf. 1999,* E. Lugscheider and P.A. Kammer, eds., DVS-Verlag, Düsseldorf, 1999, pp. 122-27.
9. W. Schedler: *Hardmetals for the Practical Expert,* VDI-Verlag, Düsseldorf, 1988 (in German).
10. K. Kirner: *Schweissen Schneiden,* 1989, vol. 41 (11), pp. 583-86 (in German).
11. P. Stecher, F. Benesovsky, and H. Nowotny: *Planseeber Pulvermet,* 1964, vol. 12, pp. 89-95 (in German).
12. V.N. Eremenko, T.Y. Velikanova, and A.A. Bondar: *Dokl. Akad. Nauk Ukrainskoj SSR, Ser. A, Fiz.-Mater. Nauki,* 1986, No.11, pp. 74-78 (in Russian).
13. J. Hinnüber and O. Rüdiger: *Arch. Eisenhüttenwes.,* 1953, vol. 24 (5-6), pp. 267-74 (in German).
14. E. Rudy and Y.A. Chang: in *5th Plansee-Seminar "De re Metallica" 1964,* F. Benesovsky, ed., Metallwerk Plansee AG, Reutte/Tyrol, 1965, pp. 786-818.
15. H. Holleck: *Binary and Ternary Carbide and Nitride Systems of the Transition Metals,* Gebrueder Borntraeger, Berlin-Stuttgart, 1984 (in German).
16. W. Köster and F. Sperner: *Arch. Eisenhüttenwes.,* 1955, vol. 26 (9), pp. 555-59.
17. A. Kusoffsky and B. Jansson: *CALPHAD,* 1997, vol. 21 (3), pp. 321-33 (in German).
18. V. Chabretou, O. Lavergne, S. Lay, C. Allibert, and L. Pontonnier: in *Proc. 1998 Powder Metallurgy World Congress & Exhibition,* European Powder Metallurgy Association, Shrewsbury, United Kingdom, 1998, vol. 4, pp. 146-51.
19. H. Suzuki and K. Tokumoto: *J. Jpn. Soc. Powder Powder Metall.,* 1984, vol. 31, pp. 56-59 (in Japanese with English abstract).
20. J. Zackrisson, B. Jansson, G.S. Upadhyaya, and H.-O. Andrén: *Int. J. Refract. Met. Hard Mater.,* 1998, vol. 16 (4-6), pp. 417-22.
21. R. Motitschka, P. Ettmayer, and E. Kny: in *Proc. 12th Int. Plansee Seminar,* H. Bildstein and H. Ortner, eds., Metallwerk Plansee, Reutte, 1989, vol. 2, pp. 863-68 (in German).
22. P. Ettmayer: *Mater. Sci.,* 1989, vol. 19, pp. 145-64.
23. O. Knotek, H. Seifahrt, and R. Kieffer: *Arch. Eisenhüttenwes.,* 1968, vol. 39 (11), pp. 869-75 (in German).
24. Y. Masumoto, S. Imasoto, and K. Tokumoto: *Nippon Tungsten Rev.,* 1986, vol. 19, pp. 19-25.
25. E. Kny and L. Schmid: *Int. J. Refract. Met. Hard Mater.,* 1987, vol. 6 (3), pp. 145-48.
26. D. Banerjee, G.K. Lal, and G.S. Upadhyaya: *J. Mater. Eng. Performance,* 1995, vol. 4 (5), pp. 563-72.
27. A.J. Ninham and A.V. Levy: *Wear,* 1988, vol. 121, pp. 347-61.
28. J.M. Guilemany and J.S. Molino: in *Proc. 1998 Powder Metallurgy World Congress & Exhibition,* European Powder Metallurgy Association, Shrewsbury, United Kingdom, 1998, vol. 4, pp. 179-84.
29. P.A. Webb, C. Orr, R.W. Camp, J.P. Olivier, and Y.S. Yunes: *Analytical Methods in Fine Particle Technology,* Micromeritics Instrument Corporation, Norcross, GA, 1997.
30. L.-M. Berger: in *TS'93: Thermische Spritzkonferenz '93,* DVS Berichte, Dt. Verlag für Schweißtechnik, Düsseldorf, 1993, vol. 152, pp. 348-50.
31. V.A. Tracey: *Int. J. Refract. Met. Hard Mater.,* 1992, vol. 11 (3), pp. 137-49.
32. W. Yin: "Influence of Dissolved Metals and Carbides on the Physical, Chemical and Mechanical Properties on the Common Hardmetal Binders Nickel and Cobalt," Ph.D. Dissertation, Vienna University of Technology, Austria, 1981 (in German).
33. A. Karimi, and C. Verdon: *Surf. Coating Technol.,* 1993, vol. 62, pp. 493-98.
34. J.M. Guilemany and J.M. De Paco: in *Proc. United Thermal Spray Conf.,* 1999, E. Lugscheider and P. A. Kammer, eds., DVS-Verlag, Düsseldorf, 1999, pp. 765-70.
35. J. Lammer and F. Benesovsky: *Planseeber. Pulvermet.,* 1973, vol. 21, pp. 18-33 (in German).
36. L.-M. Berger, P. Vuoristo, T. Mäntylä, and W. Gruner: in *Thermal Spray: Meeting the Challenges of the 21st Century,* C. Coddet, ed., ASM International, Materials Park, OH, 1998, pp. 75-82.